

Novel Progress in the High-sensitivity Heterolithic Ring Laser Gyroscope Technology

R. Santagata^{1,2}, J. Belfi², N. Beverini^{2,3}, G. Carelli^{2,3}, A. Di Virgilio², E. Maccioni^{2,3}
and A. Simonelli^{2,3,4}

¹*Department of Physics, University of Siena, Via Roma 56, Siena, Italy*

²*INFN Section of Pisa, Largo Bruno Pontecorvo 3, Pisa, Italy*

³*Department of Physics, University of Pisa, Largo Bruno Pontecorvo 3, Pisa, Italy*

⁴*Department of Earth Sciences, University of Pisa, Via Santa Maria 53, Pisa, Italy*

1 ABSTRACT

The sensitivity achieved by large ring laser gyroscopes opens the perspective to observe in an Earth-located laboratory extremely small effects expected from fundamental theories of physics. The next-generation sensor that could provide the required accuracy is a multiaxial heterolithic ring laser actively stabilized via a precise external diagnostic of circulating laser beams path.

Here we report about the research activities and recent progress toward the development of a large frame He-Ne triaxial sensor with an ultimate accuracy of 10^{-11} , in order to detect the relativistic Lense-Thirring effect related to the Earth rotating mass. The actual activity is focused on the control of the systematic errors related to the fluctuation of the cavity geometry and the laser active medium parameters. In this work we will discuss in details only the first issue, to which my PhD studies are mainly dedicated.

2 RESEARCH PROBLEM AND OUTLINE OF OBJECTIVES

Ring lasers gyroscopes (RL) are inertial sensors able to measure absolute rotations (Stedman G.E., 1997); if they are placed at rest in a ground-located laboratory, the measured rotation is that of our planet $\vec{\Omega}_{\oplus}$.

Lense-Thirring effect, predicted by Einstein's Theory of General Relativity, consists in a dragging of the local inertial frame of reference caused by the perturbation of the local metrics in the proximity of a spinning massive body like Earth (Lense J. and Thirring H., 1918). This implies that the Earth rotation rate measured against the "fixed-stars" inertial frame differs from the rotation rate measured

in the laboratory frame. In the low field approximation, the dominant correction terms are given by a geodetic term (or gravito-electric effect) due to the gravitational red-shift, and by a dragging term proportional to the angular momentum, known as Lense-Thirring effect or gravito-magnetic effect. On the Earth surface both corrective effects are of the order of 1 part in 10^9 of $\vec{\Omega}_{\oplus}$, but while the geodetic term is radially directed, the dragging one has a dipolar shape.

This has been already observed as global effect on orbiting satellites, as GRAVITY-B experiment and LAGEOS orbital data analysis (Everitt C.W.F. et al., 2011) (Ciufolini I., 1986). The experiment named GINGER (Gyroscopes IN General Relativity) (Bosi F. et al., 2011) (Di Virgilio A. et al., 2014) aims at measuring, for the first time in a ground-based laboratory, the Lense-Thirring effect locally, by using an array of large RLs placed in a Earth-based laboratory.

The requirements needed to make this possible can be clearly understood examining the sensor response. The basic setup of a RL is made up of a stable ring optical cavity along which an active medium, typically a He-Ne mixture, is placed (figure 1); two laser beams are generated and propagate in opposite directions along the loop. A Sagnac beat frequency of the circulating beams is measured (Sagnac G., 1913):

$$f_S = \frac{4\vec{A} \cdot \vec{\Omega}}{\lambda P}, \quad (1)$$

where $\vec{\Omega} = \vec{\Omega}_{\oplus} + \vec{\Omega}'$ is the rotation relative to the local Lorentz inertial frame (being $\vec{\Omega}'$ any correction term), \vec{A} is the area vector enclosed by the ring optical path P and λ is the wavelength of the laser.

The sensitivity limit of a RL is given by the shot-noise:

$$\Omega_{sn} = \frac{vP}{4AQ} \sqrt{\frac{hf}{P_{out}T}}, \quad (2)$$

where v is the velocity of the laser beam along the cavity, Q is the quality factor of the resonator, h the Planck constant, P_{out} the detected optical power and T the measuring time.

From equation 1 two important features follow: the dependence of Sagnac frequency f_S on the laser path geometry via the scale factor $k_S = 4A/\lambda P$, and the scalar nature of the sensor output, being measured only the projection of the velocity vector $\vec{\Omega}$ on the enclosed area \vec{A} .

The development of a high sensitivity RL requires:

- a large frame structure. To increase the size of the ring cavity, in fact, implies to increase the signal to noise ratio (SNR), being the signal proportional to the ratio A/P via the scale factor, and the shot noise of the sensor proportional to P via the quality factor Q .
- a high-Q resonator ($> 10^{11}$ and higher). Low-loss 'five-9s quality' supermirrors must be used.
- a multi-axial system of RL, in order to reconstruct the modulus of the Earth rotational vector and compare the Earth rotation rate measured locally with the one provided by IERS (International Earth Rotation and Reference Systems Service). Otherwise, an absolute calibration of the RL orientation at a level of 0.1 nrad would be needed.
- to reduce the instrumental drift in the measurement of rotation rate to less than Ω'/Ω_{\oplus} . This needs a long-term strict control on the fluctuation of laser active medium, cavity geometry and, in a RLs array, of relative dihedral angles.
- to reduce all the sources of Earth-surface and environmental noise, installing the detector in a very stable geological environment, well coupled to the solid rock, in a low environmental noise laboratory, possibly located underground.

3 STATE OF THE ART

To this day, the best RL is the Grossring 'G', located at the Geodatisches Observatorium in Wettzell, Bavaria (Schreiber K.U. et al., 2009) (Schreiber K.U. et al., 2011). It has achieved a resolution better than 5×10^{-13} rad/s with an integration time of few hours, becoming of geodetic interest for measuring short-term fluctuation, with periods of hours to days, in Earth rotation.

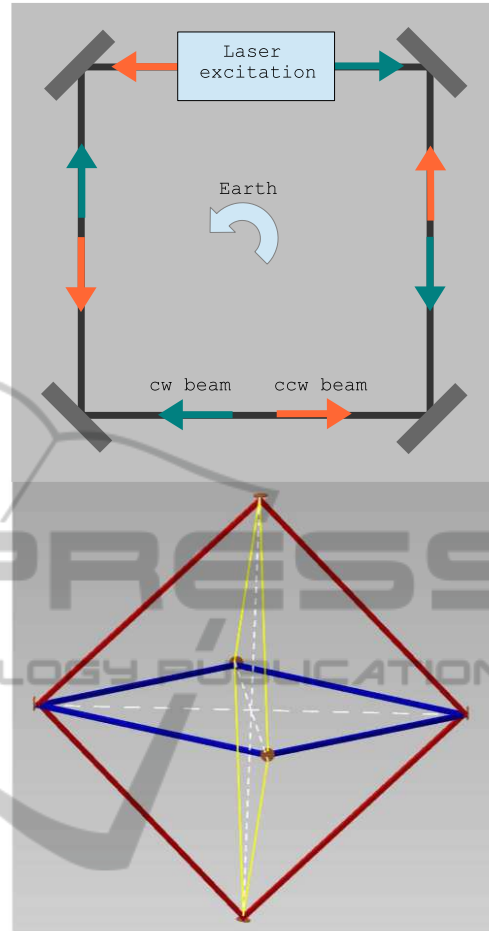


Figure 1: Ring laser gyroscope. Above: setup of a square RL. Below: triaxial sensor made of 6 mirrors. Each couple of opposite mirrors is shared between two rings.

This stability record is mainly due to its building material that allows a strong passive stabilization of the optical cavity. G, in fact, is a semi-monolithic device made in Zerodur, a glass ceramic with an especially small thermal expansion, high mechanical stability and consistency of shape and length. Four bars are rigidly connected to a base plate forming the edges of a square 4 m length in side; spherical supermirrors are attached to the face sides of the bars by molecular adhesion, ensuring a stable vacuum seal. It is kept in an underground controlled room and equipped with an active control of the cavity perimeter that stabilizes the circulating laser beams frequency against an optical frequency reference.

Albeit G resolution is very close to that required to detect the relativistic effects on rotation, its design can't be used to develop a large frame RLs array, since larger monolithic blocks of Zerodur are not available. The next-generation RL able to detect tiny effects, as Lense-Thirring effect, has a heterolithic

multi-axial design equipped with a precise diagnostic system of laser beam path deformation, in order to stabilize the scale factor k_S better than 10^{-10} .

Recent studies and experimental activities made in this context on the middle-size heterolithic RL 'G-Pisa' (Belfi J. et al., 2012), have motivated the design of the GINGER device. It consists in a triaxial system of large square heterolithic RLs arranged in an octahedral structure (figure 1). A suitable location for this device could be the underground facility of LNGS (Laboratori Nazionali del Gran Sasso - Italy).

To accomplish GINGER's goal needs a control of the systematic errors related to the fluctuation of the cavity geometry and the laser active medium parameters. As regards the last issue, a set of spectroscopic diagnostic of the active medium parameters and an off-line denoising method that, based on the Kalman filter approach, subtracts from the raw Sagnac data the systematic effects induced by the non-linearity of the RL dynamics, has been developed (Beghi A. et al., 2012) (Cuccato D. et al., 2014). In the following, we'll discuss mainly about the first research field.

4 RING CAVITY GEOMETRY CONTROL

The measure of Lense-Thirring effect in a ground-based laboratory requires a stabilization of the scale factor k_S better than 10^{-10} . This implies an accuracy on mirror positions better than 1 nm and on the ring cavities relative orientation better than 1 nrad.

In a square RL, a so strict control on mirror positions can be reduced if the absolute length of the diagonal cavities is stabilized in addition to the perimeter one, so that the closed optical path shape is that of a regular square. Our theoretical and numerical studies are reported in detail in Ref.(Santagata R. et al., 2014). We showed that if the length of the two diagonals are locked to the same value, the perturbations to the mirror positions affect only quadratically the ring laser scale factor. This constraint reduces the mirror position fluctuation at a level of 1 part in 10^{10} , even if the two lengths are stabilized to values that differs at a micrometric scale.

These results motivated the design of GP2 (Di Virgilio A. et al., 2014), an intermediate prototype of GINGER specifically devoted to test the active control strategies and, in particular, to implement the length stabilization of the diagonal resonators by means of optical interferometry. In addition to it, the GINGERino prototype has also been developed last year (Di Virgilio A. et al., 2014); it is especially birth

to analyze the seismic noise at LNGS location, but also to tryout the SNR improvement of a larger cavity.

The optical setup of both devices consists in four supermirrors each one contained in a steel holder placed at the corner of a granite support fixed on a concrete base. Steel pipes connected by the mirror holders define the vacuum chamber that encloses the optical path of the circulating beams along a square loop. The vacuum chamber is filled with a mixture of He-Ne and the capacitive discharge for laser excitation, consisting in a pyrex capillary, is located in the middle of a side of the cavity. The laser frequency is stabilized with respect an optical frequency reference in order to actively control the ring cavity perimeter.

In section 5 GP2 and GINGERino prototype are described. To stabilize the absolute length of diagonal resonators we worked out an interferometric metrology technique and we tested it on two Fabry-Perot cavities simulating the ring diagonals on an optical bench. We report some details about this work, whose results has been published in Ref.(Belfi J. et al., 2014), in section 6. Finally, in section 7 expected outcome and future perspectives are discussed.

5 METHODOLOGY

5.1 GP2

5.1.1 Optical Setup

GP2 is the seed device for the next generation heterolithic active-stabilized RLs. It has been designed in order to gain a long term stability and accuracy of the scale factor, via a precise control of the systematic errors related to the fluctuation of the cavity geometry and the active medium parameters. In particular, it is dedicated to implement a length stabilization of the diagonal cavities using optical interferometric techniques.

Figure 2 shows a drawing of GP2 (above) and its installation in a clean room at INFN Pisa laboratories in March 2014 (below). The granite slab whereon the cavity is placed is oriented along the local latitude in order to maximize the Sagnac signal and minimize the orientation errors on scale factor. The four mirrors holders are placed at the corner of a square granite slab and the vacuum chamber encloses the beam optical path along a square loop 1.60 m length in side. Figure 3 shows a preliminary Sagnac spectrum; a Sagnac frequency of 184 Hz has been observed, as expected.

To check the quality factor $Q = 2\pi f\tau$ of the laser

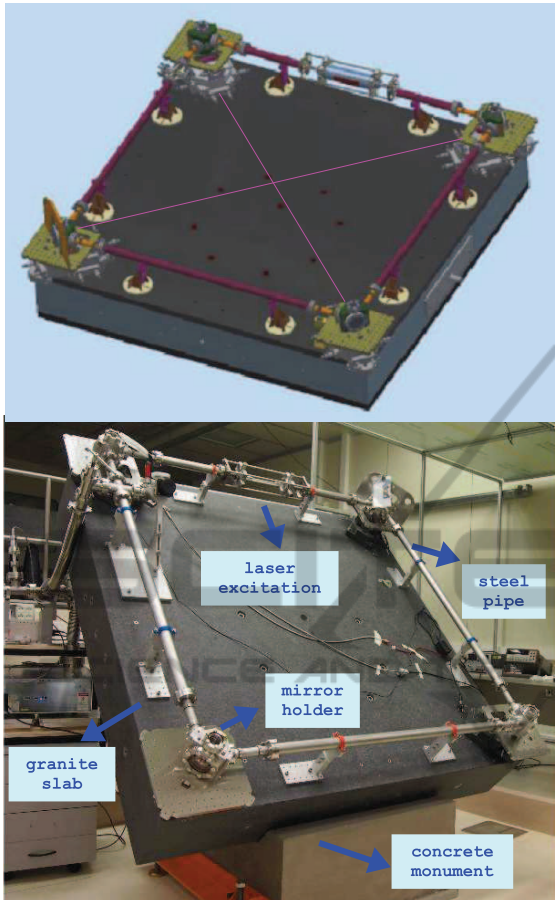


Figure 2: GP2 ring laser gyroscope. Above: drawing of the design. Below: The sensor installed at the clean room of INFN Pisa section laboratory (March 2014).

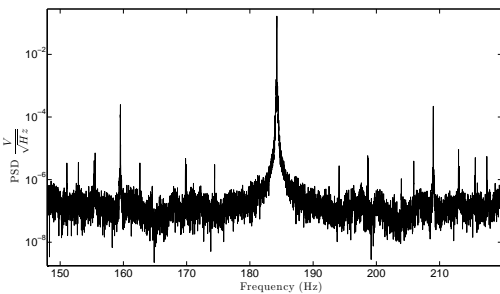


Figure 3: Power spectral density of GP2 data. The Sagnac response peak at 184 Hz is observed.

cavity we made a ring-down time τ measurement of the laser by short-circuiting the discharge capacitor. In figure 4 we report the laser intensity decay trace acquired by the oscilloscope. Fitting to data the exponential function $I = I_0 + Ce^{-t/\tau}$, where I_0 is the initial intensity and C a numerical constant, we have obtained a measure for the ring-down time $\tau = 154.4 \pm 0.5 \mu\text{s}$. This corresponds to a quality cavity factor $Q = 4.6 \times 10^{11}$

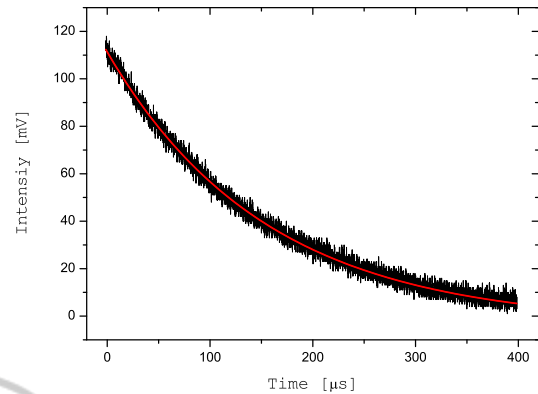


Figure 4: Ring-down time measurement of GP2 laser cavity. Black line: trace of laser intensity decay acquired by the oscilloscope. Red line: exponential fit of data points. Fit results: $\tau = 154.4 \pm 0.5 \mu\text{s}$; $I_0 = -3.35 \pm 0.10 \text{ mV}$; $C = 114.63 \pm 0.14 \text{ mV}$.

5.1.2 Mechanical Expedients for Diagonal Cavities Stabilization

The slab whereon the holders are mounted is made of precise black granite, a rock well suited for metrology application for his long term thermal and dimensional stability, high flatness accuracy, high bending strength and insensitivity to mechanical overloading. It has been machined with a precision better than $10 \mu\text{m}$ to guarantee a preliminary well positioning of the corner mirrors.

To implement the diagonal absolute length stabilization, by using the experimental technique described in section 6, the GP2 vacuum chamber has been designed in order to give access to the diagonal resonators by enclosing the path of two external laser beams along these, as well as the perimeter path of the counter-propagating beams. These two additional chamber parts, schematically indicated in the above of figure 2, will be installed in the near future.

A high finesse of the Fabry-Perot cavities is guaranteed by a special mirror coating that ensures a reflectivity of about 99.9% at normal incidence, in addition to a reflectivity $> 99.999\%$ at 45 deg angle of incidence.

The design of mirror holders, whose most important features are showed in figure 5, is of key importance in view of the diagonal cavities use.

The mirrors are accessible through big optical transparent windows installed parallel to them on the holders. The window allows the circulating monobeams to exit the cavity and to be monitored; an external optical setup detects the beat frequency. In addition, it consents to an external He-Ne laser source hitting it at normal incidence to enters into the diagonal resonators, as showed in the below of figure 5.

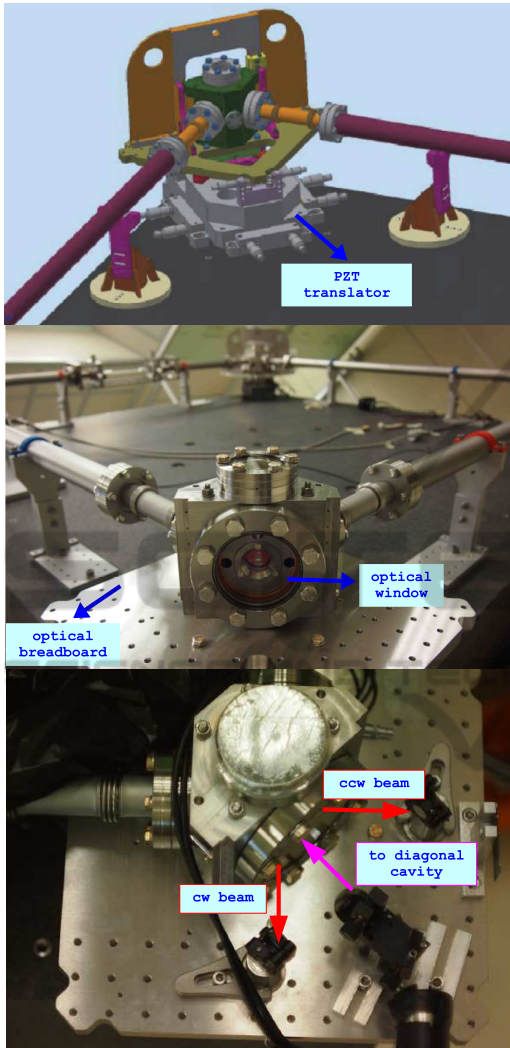


Figure 5: GP2 Mirror holders. Above: drawing of the holder design; the piezo system is shown. Middle: picture of the holders installed on the granite slab. The big optical transparent window allowing the optical access to corner mirror is shown. Below: detail of holder. The optical setup needed to combine the circulating beams is also shown. The combiner is mounted on a small breadboard and consists in two high-reflection dielectric mirrors 0.5 inch in size. For the detection of the beat frequency, a photodiode integrated with an interference filter is used. The three allowed directions (monobeams exiting the cavity and external laser source entering in the diagonal resonator) are pointed out.

To get a regular square cavity by a dynamic control, the mirror holders are equipped with a piezo nano-positioning system. Since each mirror displacement can be described as a variation in the space of the position of its curvature center, the geometry of the optical path along the square loop is completely determined by the 12 centres coordinates (12 degree of freedom). In Ref.(Santagata R. et al., 2014) we have

defined the eigenvectors basis of the cavity deformations, identified the rigid body motion of the cavity, and then classified the residual 6 optical cavity deformations once the diagonal lengths are stabilized. For this reason, in GP2 a total of 6 piezo-electric transducers (PZT) is used. One holder is provided with a 3-axial PZT, while the other three with a 1-axial PZT along the diagonal.

The piezo system has a dynamic range of $80 \mu\text{m}$. To have an estimate of the displacement response, we made a calibration of the 1-axial translators by measuring the displacement induced by an applied voltage. The PZT calibration data are plotted in figure 6; a second order polynomial fit provide a displacement constant mean value of $(7.4 \pm 0.6) \mu\text{mV}^{-1}$ for the mirrors mounted on the north side of the RL, and $(9.2 \pm 0.4) \mu\text{mV}^{-1}$ for the mirrors mounted on the south side.

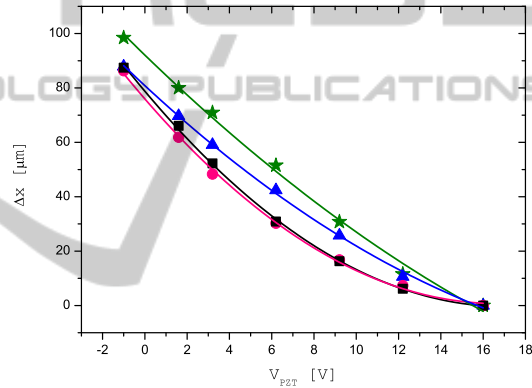


Figure 6: PZT calibration data. The displacement data induced by an applied voltage are plotted for each 1-axial piezo moving the mirror holder along the ring cavity diagonal. Positive variation means displacement toward the center of the ring. A second order polynomial $\Delta x = AV_{PZT} + BV_{PZT}^2$ is fitted to data. From top to bottom: corner 4 (green line), $A_1 = (-9.3 \pm 0.2) \mu\text{mV}^{-1}$, $B_1 = (0.271 \pm 0.013) \mu\text{mV}^{-2}$; corner 3 (blue line), $A_2 = (-9.0 \pm 0.3) \mu\text{mV}^{-1}$, $B_2 = (0.269 \pm 0.018) \mu\text{mV}^{-2}$; corner 1 (black line), $A_3 = (-7.2 \pm 0.3) \mu\text{mV}^{-1}$, $B_3 = (0.132 \pm 0.017) \mu\text{mV}^{-2}$; corner 2 (magenta line), $A_4 = (-7.5 \pm 0.5) \mu\text{mV}^{-1}$, $B_4 = (0.10 \pm 0.04) \mu\text{mV}^{-2}$.

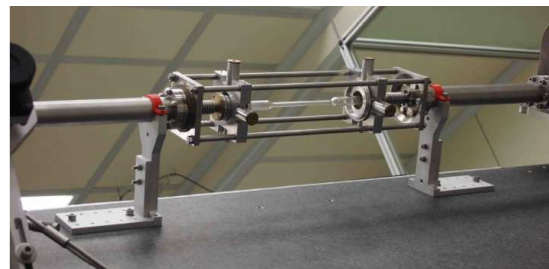


Figure 7: Pyrex tube for the excitation of the He-Ne plasma.

A fine control of the laser beam path requires also a well positioning of the discharge system. To this aim, the pyrex capillary is linked to the steel pipes by means of a cage system equipped with a micrometric regulation of its position and tilt. A detail of the cage system is reported in figure 7.

5.2 GINGERino

GINGERino is an evolution of G-Pisa RL. While the fundamental purpose of G-Pisa was to acquire the expertise on the operation of a large frame RL, GINGERino is its upgrading that has been placed in the LNGS underground laboratory in order to test the adequacy of the site to guest the GINGER apparatus.

The 1400 m thick rock of the central massif of Gran Sasso constitutes a natural shielding against all the sources of noise coming from the surface activities. The underground environment guarantees in addition a high stability of the local environmental parameter such as pressure, temperature and humidity. At the same time, the operation of GINGERino in a low local noise laboratory could give the possibility to detect geodetic signals (Polar motion, Chandler wobble, tidal effects,...) and seismic signals (S-wave phase velocity,...) for which a sensitivity of $10^{-9} - 10^{-13}$ rad/s is sufficient. The analysis of the rotational seismic noise and its correlation with classical seismometer signals will be carried out by researchers of INGV (Italian National Institute of Geophysics and Vulcanology). A comparison with G measurements would be very interesting in the case of non-local effects, such as tele-seismic events.

Figure 8 shows a drawing of GINGERino (above) and its installation in the Node A of the so-called "interferometric tunnel" at LNGS in October 2014 (below). This gallery is in the northern part of the laboratories, away from the 3 large Halls hosting the main experiments and so away from the principle sources of daily human activity noise. As in GP2, the square optical cavity consists in supermirrors placed inside corner holders connected by steel pipes. Holders and pipes are those of the first prototype, G-Pisa, increased in size to get a length of side of 3.60 m. A Sagnac frequency of 280 Hz has been observed, as shown in figure 9.

The cavity is mounted on a granite slab installed on a concrete monument well connected to the rock floor. To reduce the weight of the apparatus and simplify its installation in the cave, the slab consists in four arms that has been inserted in loco into a central square granite block. To improve the mechanical stability of the discharge system, the capillary holder is fixed on a breadboard sustained by four concrete pil-

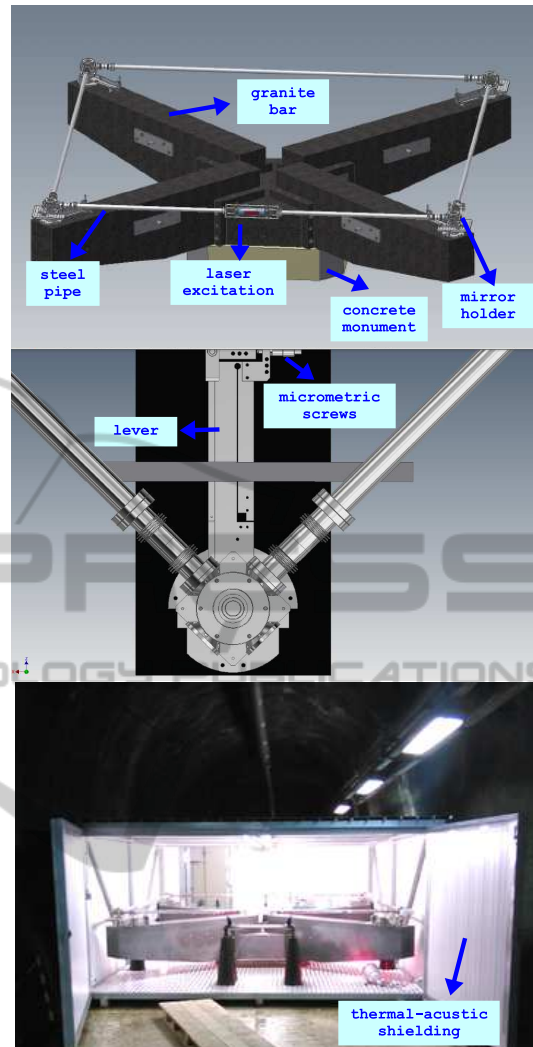


Figure 8: GINGERino ring laser gyroscope. Above: drawing of the design. Middle: detail of the lever system controlled by micrometric screws used to align the ring cavity. Below: installation at LNGS underground facility (October 2014). The thermal-acoustic shielding enclosing it is shown.

lar; two of these sustain each cavity side also. The mirrors, rigidly connected to the holders, can be tilted to align the cavity by means of levers controlled by micrometric screws (figure 8). Only two of the four mirrors are equipped with a monodimensional micrometric PZT that, mounted under the holders, move the mirror along one diagonal of the square cavity. This makes possible only a dynamic control of the beam path perimeter, that is keep constant against an optical frequency standard.

The apparatus is enclosed by a thermal-acoustic shielding and the laboratory is warm up making use of heat lamps symmetrically arranged around the device. To give an assessment about the room-temperature stability and homogeneity, we attached a

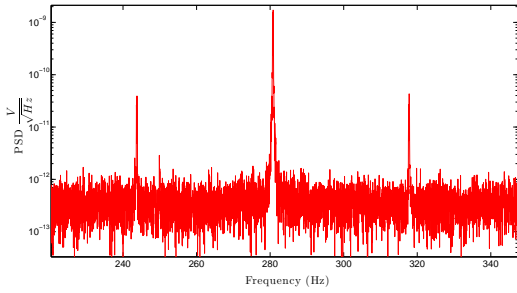


Figure 9: Power spectral density of GINGERino data. The Sagnac response peak at 280.05 Hz is observed.

platinum RTD (Resistance Temperature Device) sensor attached to each corner of the steel cavity structure. Throughout 5 days, a maximum gradient of $0.5\text{ }^{\circ}\text{C}$ between the mean values of temperature in two different corners is observed; the fluctuation around each mean value, measured using standard deviation, is of $0.04\text{ }^{\circ}\text{C}$.

6 STAGE OF THE RESEARCH. ABSOLUTE LENGTH STABILIZATION OF THE SQUARE RL DIAGONAL CAVITIES

6.1 Measurement Principle

To stabilize the absolute length of a square RL diagonal resonators with respect to an interrogating high-stability laser we worked out an interferometric metrology technique and we tested it on two Fabry-Perot cavities simulating the ring diagonals on an optical bench. The technique we used is based on an accurate frequency measurement of the resonant longitudinal mode and an univocal determination of the interference order (Belfi J. et al., 2014). For a TEM_{00} laser mode of order n resonating in a cavity formed by two concave spherical mirrors of radius R , the resonance frequency f_n is given by:

$$f_n = \frac{v}{2L} \left[n + \frac{1}{2\pi} (\Psi_R + \Phi_n) \right] \quad (3)$$

where v is the speed of light inside the cavity and L is the distance between the mirrors. Ψ_R and Φ_n are two phase corrections due respectively to the phase accumulation along the direction of laser beam propagation (Guoy phase) and the dielectric mirror phase shift upon reflection; these two terms can be evaluated from the knowledge of R and the mirror reflectivity curve.

To measure L with a 10^{-10} accuracy needs to measure f_n with the same accuracy and define univocally the integer n . This can be done locking the cavity resonance to the laser carrier frequency (carrier lock) and the phase modulation frequency to a harmonic m of the free spectral range (sideband lock). We get the two error signals required to implement the double-lock modulating the laser source with a electro-optic modulator (EOM) driven by three independent modulation frequencies: the first modulation at frequency ω_A provides the Pound-Drever-Hall signal for carrier lock; the second modulation at frequency ω_B provides the lock-in amplifier error signal; the latter is referred to a third modulation at ω_C for shifting the the FSR detection down to few tens kHz.

6.2 Apparatus and Experimental Procedure

The apparatus we developed is shown in figure 10. The laser source is a 10mW diode laser emitting at 633 nm. A high spectral purity is gained referring it to an optical reference frequency provided by a $100\text{ }\mu\text{W}$ He-Ne laser frequency stabilized on the saturated absorption line R-127 11-5 of Iodine. This is achieved implementing a light amplifier based on injection-locking. The features of the laser source are summarized in table 1.

The Fabry-Perot resonators simulate the ring cavity diagonals on an optical bench. They are formed by curved mirrors mounted on holders connected by Invar spacers; the output mirror is equipped with a piezoelectric translator to implement the feedback correction to the cavity length. The parameters of the two resonators are reported in table 2.

The injection-locked laser beam, after being triple-phase-modulated by a single fiber-coupled EOM, enters into the two Fabry-Perot cavities. The reflected beam, detected by a photodiode and splitted by a two way power divider, is demodulated according to a standard Pound-Drever-Hall scheme (first one way) and by a digital lock-in amplifier (second one way) in order to recover the carrier error signal ϵ_0 and sideband error signal $\epsilon_{S(1,2)}$. These are used to apply corrections to the cavity PZTs and to a Voltage Controlled Oscillator (VCO) generating the sidebands at $m \cdot FSR$.

Table 1: Injection-locked laser source features.

Wavelength	633 nm
Output power	10 nW
Allan deviation	10^{-11} (at 100 s)

The carrier feedback loop locks the two cavities

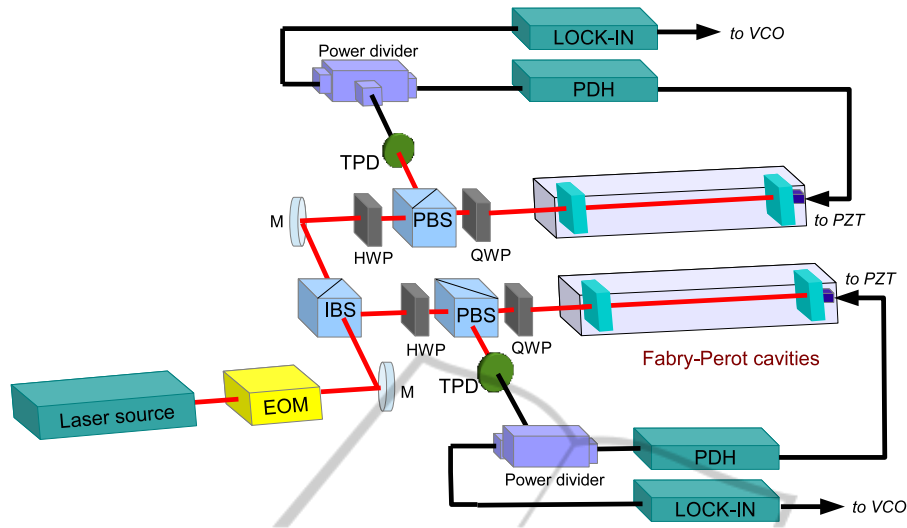


Figure 10: Conceptual scheme of experimental apparatus. A more detailed scheme is reported in (Belfi J. et al., 2014). The laser source block represents the injection locking setup. The PDH stage represents the module for locking with Pound-Drever-Hall scheme, while the Lock-in one includes the circuit for the digital lock-in amplifier phase-detection. EOM: Electro-Optic Modulator. IBS: Intensity Beam Splitter. PBS: Polarizing Beam Splitter. HWP: Half Wave Plate. QWP: Quarter Wave Plate. TPD: Transimpedance Photodiode. PZT: Piezoelectric Transducer. VCO: Voltage Controlled Oscillator.

Table 2: Optical parameters of cavities test-bench. They have an identical mechanical setup, but the reflectivity of the input mirror are different leading to different Full Width at Half Maximum (FWHM) width of the resonator resonances. Left: Cavity 1. Right: Cavity 2.

L	1.32 m
R	4 m
FSR	113 MHz
r_{in}^2	0.988; 0.997
r_{out}^2	0.999; 0.999
$Finesse$	480; 1570
$FWHM$	225 kHz; 54 kHz

resonance frequencies to the same laser carrier frequency. The sideband feedback loop processes the error signals $\varepsilon_{S(1,2)}$ by a LabView program running on a PC and locks by turns the VCO frequency alternatively to $m \cdot FSR_1$ or $m \cdot FSR_2$ until the two interference orders $n_{1,2} = \omega_0 / 2\pi \cdot FSR_{1,2}$ are determined with the required precision. A microwave frequency counter connected to the auxiliary output of the VCO acquires with a gate-time of 1 s the $FSR_{1,2}$ data.

6.3 Results

A gaussian fit of the FSR data provides an estimate for the central frequency of the two cavities f_{c1} , f_{c2} and the standard deviation about these σ_1 , σ_2 . The frequency data are then used to calculate the distribution of the mode number difference:

$$n_D = \frac{\omega_0}{2\pi} \left(\frac{1}{FSR_2} - \frac{1}{FSR_1} \right), \quad (4)$$

whose standard deviation σ_{n_D} is finally used to estimate the length difference $\delta D = (\lambda/2) \cdot \sigma_{n_D}$. The mode difference n_D should be an integer univocally determined; in this case the error on the length difference between the two diagonals is ultimately limited by the uncertainty on the laser wavelength.

Since the optical frequency is stabilized at the level of 1 part in 10^{11} , the uncertainty on the mode number difference σ_{n_D} is given by the uncertainty $\Delta FSR_i / FSR_i$, $i = 1, 2$. In table 1 we report the results of the analysis of the frequency data acquired modulating at $\omega_B = 6 \times FSR$. The FSR mean values are determined to few parts in 10^7 , and the corresponding mode number difference with an uncertainty of 1.6. This is finally used to estimate the length difference $\delta D = (\lambda/2) \cdot \sigma_{n_D}$, that with our set-up is 500 nm (Belfi J. et al., 2014). Note that the FSR uncertainty

Table 3: Experimental results of cavities test bench.

f_{c1}	681211560 Hz
σ_1	230 Hz
f_{c2}	680000798 Hz
σ_2	140 Hz
n_D	7427
σ_{n_D}	1.6

decreases as cavity finesse increases. We have studied also the dependence of σ_i on harmonic m , and our ex-

perimental results suggest an improvement in FSR determination as m^{-1} . These considerations are of relevance in view of the implementation of the technique in GP2.

7 EXPECTED OUTCOME

The primary expected outcome of the future work is to make the most of the developed expertise to run GP2 with the target geometrical stability of 1 part in 10^{10} . We intend to implement the length stabilization of the GP2 diagonal cavities by using the experimental setup described in section 6 with some adaptations.

First, in the test bench experiment the laser source was modulated by a single EOM and a single VCO was alternatively locked to the resonances of the two cavities. To ensure a long-term run of the RL with the diagonal stabilization constraint, we plan to divide the laser beam with a bifurcated fiber and to modulate the resulting two beams by using two identical EOMs.

Moreover, we have to take into account that an unavoidable uncertainty on the measurement of the instantaneous length of a cavity is the acoustic. Since in a RL the mirror position actuators have a limited bandwidth (< 100 Hz) due to mirror holders inertia, a possible solution is to lock the laser to the diagonal cavities using an acousto-optic modulator (AOM) that compensates this noise by shifting the laser frequency.

The GP2 diagonal resonators have a FSR of 66 MHz and a finesse of $\simeq 3000$. In this case, operating with a modulation frequency $\omega_B = 1$ GHz (EOM bandwidth cut-off) we expect to be able to determine the mode number difference univocally, i.e. with an uncertainty less than 1.

Furthermore, the full startup of GINGERino prototype will test the adequacy of LNGS location in terms of rotational noise and environmental stability. From its operation we foresee an improvement of SNR respect to G-Pisa of about a factor 7, being the increase in SNR more than quadratic with the ring side size, as explained in section 2. In this case, geodetic and microseismic signals will be detected, and we plan to compare the acquired data with those provided by G ring laser and by different rotational seismology observatories.

If we achieve these results, the potentialities of an heterolithic large RL for the detection of tiny effects, as Lense-Thirring effect, will be experimentally demonstrated, and a first important step toward GINGER will be taken.

REFERENCES

- Beghi A. et al. (2012). Compensation of the laser parameter fluctuations in large ring-laser gyros: a Kalman filter approach. *Appl. Opt.* 51, 7518-7528.
- Belfi J. et al. (2012). A 1.82 m2 ring laser gyroscope for nano-rotational motion sensing. *Appl. Phys. B* 106, 271-281.
- Belfi J. et al. (2014). Interferometric length metrology for the dimensional control of ultra-stable ring laser gyroscopes. *Class. Quant. Grav.* 31, 225003.
- Bosi F. et al. (2011). Measuring Gravitomagnetic Effects by Multi Ring-Laser Gyroscope. *Phys. Rev. D* 84, 122002.
- Ciufolini I. (1986). Measurement of the Lense-Thirring drag effect on LAGEOS and another high altitude laser ranging satellite. *Phys. Rev. Lett.* 56, 278-281.
- Cuccato D. et al. (2014). Controlling the non-linear intracavity dynamics of large He-Ne laser gyroscopes. *Metrologia*, 51, 97-107.
- Di Virgilio A. et al. (2014). A ring lasers array for fundamental physics. *Compt. rend. Phys.* 15, 866-874.
- Everitt C.W.F. et al. (2011). Gravity Probe B: Final Results of a Space Experiment to test General Relativity. *Phys. Rev. Lett.* 106, 221101.
- Lense J. and Thirring H. (1918). Über den Einfluss der Eigenrotation der Zentralkörper auf die Bewegung der Planeten und Monde nach der Einsteinschen Gravitations theorie. *Phys. Z.* 19, 156-163.
- Sagnac G. (1913). L'ether lumineux demontre par l'effet du vent relatif d'ether dans un interferometre en rotation uniforme. *Comp. Rend.* 157, 708.
- Santagata R. et al. (2014). Optimization of the geometrical stability in square ring laser gyroscopes. *arXiv:1411.2585*.
- Schreiber K.U. et al. (2009). The Large Ring Laser G for Continuous Earth Rotation Monitoring. *Journal of Pure and Applied Geophysics*, 166 1485.
- Schreiber K.U. et al. (2011). How to Detect the Chandler and the Annual Wobble of the Earth with a Large Ring Laser Gyroscope. *Phys. Rev. Lett.* 107, 173904.
- Stedman G.E. (1997). Ring-laser tests of fundamental physics and geophysics. *Rep. Prog. Phys.* 60, 615-688.